Thermopower of Amine−Gold-Linked Aromatic Molecular Junctions from First Principles

Su Ying Quek,[†] Hyoung Joon Choi,[‡] Steven G. Louie,[†,§,⊥] and Jeffrey B. Neaton[†,⊥,*]

[†]Molecular Foundry, Lawrence Berkeley National Lab, Berkeley, California 94720, United States, [‡]Department of Physics and IPAP, Yonsei University, Seoul 120-749, Korea, [§]Department of Physics, University of California, Berkeley, California 94720, United States, and [⊥]Materials Sciences Division, Lawrence Berkeley National Lab, Berkeley, California 94702, United States

ABSTRACT Using a self-energy corrected scattering-state approach based on density functional theory (DFT), we explain recent measurements of the thermopower or the Seebeck coefficient, *S*, for oligophenyldiamine−gold single-molecule junctions and show that they are consistent with separate measurements of their electrical conductance, *G*. Our calculations with self-energy corrections to the DFT electronic states in the junction predict low-bias *S* and *G* values in good quantitative agreement with experiments. We find *S* varies linearly with the number of phenyls *N*, with a gradient β^S of 2.1 μV/K, in excellent agreement with experiment. In contrast, DFT calculations without self-energy corrections overestimate both *S* and β^S (with a DFT value for β^S three times too large). While β^S is found to be a robust quantity independent of junction geometry, the computed values of *S* show significant sensitivity to the contact atomic structure—more so than the computed values of *G*. This observation is consistent with the experimentally measured spreads in *S* and *G* for amine−Au junctions. Taken together with previous computations of the electrical conductance (as reported in Quek, S. Y.; *et al.*, *Nano Lett.* 2009, *9*, 3949), our calculations of *S* conclusively demonstrate, for the first time, the consistency of two complementary yet distinct measurements of charge transport through single-molecule junctions and substantiate the need for an accurate treatment of junction electronic level alignment to describe off-resonant tunneling in these junctions.

KEYWORDS: molecular junctions · thermopower · first principles

Understanding energy conversion at the molecular level is of fundamental importance in nanoscience, and single-molecule junctions can provide highly controlled systems with which to probe electrical and thermal transport at the nanoscale.[1,2] Recent experimental demonstrations[3,4] of thermal to electric energy conversion in single-molecule junctions have sparked significant interest in their thermoelectric properties. Due to the mismatch in phonon density of states at metal−molecule interfaces, such junctions are expected to have small phonon thermal conductance.[5] Coupled with the potential of tuning both the resonance levels and degree of coupling by chemical functionalization,[6] it has been predicted that the thermoelectric figure of merit, ZT, can in principle diverge for single-molecule junctions.[5] To guide the rational design of organic−inorganic assemblies for thermoelectric applications, it is important to be able to understand and predict, from first principles, quantitative values and trends of the thermopower or the Seebeck coefficient, *S*, of single-molecule junctions and connect these quantities to their intrinsic structural and electronic properties.

The thermopower, $S = -\Delta V/\Delta T$, is a physical measure of the voltage ΔV that develops upon application of temperature gradient ΔT across a junction at zero electrical current. It is closely related to but distinct from the low-bias conductance, $G = \Delta I/\Delta V$, the amount of electrical current ΔI generated in a junction by an external voltage bias. An understanding of independent measurements of *S* and *G* for single-molecule junctions using a common theoretical framework provides opportunities to significantly deepen our understanding of the physics governing charge transport through nanoscale hybrid interfaces at the molecular level. The ability to compute both *S* and *G* values in quantitative agreement with experimentally measured values would also provide a much-needed consistency check in the field of molecular electronics.

Prior theoretical work based on a steady-state Landauer formalism[7,8] has suggested that *S* is less sensitive to the molecule−lead coupling strength (and, implicitly, contact geometry) and is therefore more amenable to theoretical predictions than *G*,[8,9] where there has been notable disagreement between theory and experiment for thiol-terminated molecules.[10−13] Other authors have argued that important non-equilibrium transient thermal effects[14] are missing from the steady-state scattering

*Address correspondence to jbneaton@lbl.gov.

Received for review October 1, 2010 and accepted December 10, 2010.

Published online December 20, 2010. 10.1021/nn102604g

picture.[7,8] In practice, it has been found that DFT approaches within the Landauer formalism using gradient corrections in the local exchange-correlation functional overestimate S,[15] while the use of certain hybrid functionals and a wide-band approximation can result in better agreement between theory and experiment for aromatic dithiol−Au junctions.[9] However, the latter approach overestimates the measured conductance by a factor of 5,[9] thus leaving open questions about the relationship between conductance and thermopower for these systems and their connection to the intrinsic properties of these junctions.

RESULTS AND DISCUSSION

In previous studies, we demonstrated that standard DFT approaches to transport can significantly overestimate the junction conductance[11,16,17] because the Kohn−Sham orbital energies place the frontier molecular resonances too close to the junction Fermi level E_F within the local density approximation (LDA) or generalized gradient approximation (GGA).[17−19] This misalignment of the molecular levels arises from many-electron self-energy effects on the carrier energies, having the same physical origin as that of the well-known DFT "band gap" problem in semiconductors.[20] In this work, we employ a DFT-based scattering-state approach that includes quasiparticle self-energy corrections to level alignment in the junction (DFT+Σ)[21,22] to compute and understand the thermopower S of single-molecule oligophenyldiamine−Au junctions as a function of the number of phenyl rings N in the molecule. Our results for S are in excellent agreement with experiment.[4] Remarkably, our computed values for G within the same DFT+Σ approach also agree very well with an *independent* experimental measurement of conductance[23] in these junctions.[21] The excellent agreement between the DFT+Σ values with these separate measurements of thermopower and conductance establish a quantitative consistency between two related but distinct transport processes through single-molecule junctions, a first in the field of molecular electronics. We further demonstrate that, for the amine−Au system, S is in fact *more sensitive* to the contact geometry than G, an effect that is not captured by assuming[8,9] a uniform DOS in the leads and that is consistent with the observed experimental spread in thermopower for the systems considered.

It has been established for amine−Au-linked molecular junctions that the amine group binds selectively to under-coordinated atop Au sites,[17] which can explain the observed statistical reproducibility of their conductance measurements.[23] On the basis of this knowledge, we model all junction geometries with oligophenyldiamine molecules bound at each amine group to atop sites of adatom and "trimer" motifs on Au(111) surfaces (Figure 1a). (Trimer motifs are partially coordinated binding sites consisting of groups of three Au atoms.) Similar geometries have yielded accurate conductance values for amine−Au and pyridine−Au-linked junctions using the DFT+Σ approach.[17,21,22,24] All of the junction geometries are fully relaxed within DFT-GGA (PBE)[25] using SIESTA.[26] Details of the DFT calculations follow ref 17. The optimized dihedral angles between phenyl rings are ~35° for all junction geometries considered.[27]

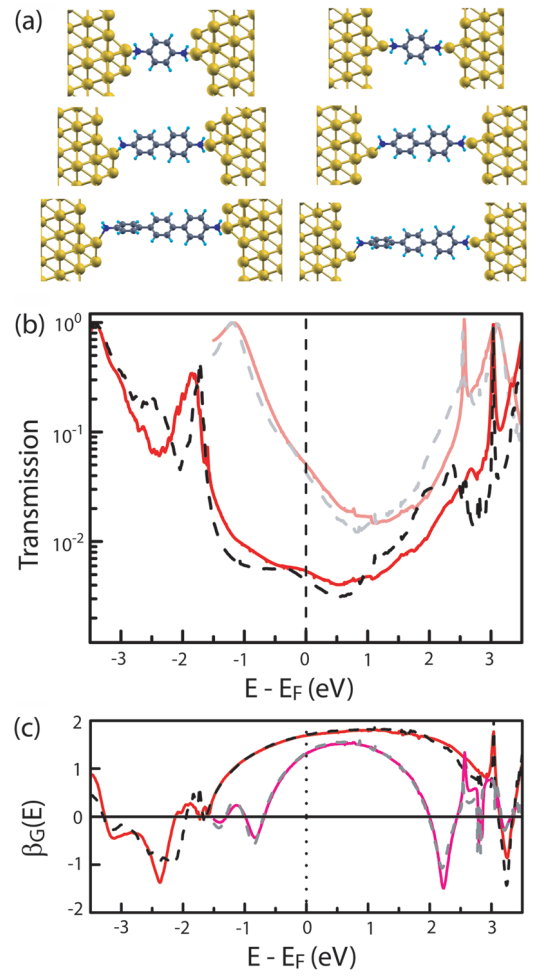

Figure 1. (a) Optimized atomic structures of oligophenyldiamine−Au junctions. Each amine group is bonded to an atop site of a Au trimer (group of three atoms) (left panel) or a Au adatom (right panel). (b) Transmission plot $\tau(E)$ for BDA−Au junctions ($N = 1$). (c) Plot of $\beta^G(E)$, obtained from the least-squares linear regression fit for ln $\tau(E)$ *versus* ln N. In (b,c), pink (gray dashed) and red (black dashed) curves represent, respectively, DFT and DFT+Σ results for trimer (adatom) junctions. The transmission in (b) is obtained using an 8 × 8 $k_\parallel$-mesh at all energies, except for the interval (−0.4, 0.4) eV for which a 24 × 24 mesh was used. Transmission plots for $N = 2$ and 3 can be found in ref 21.

Charge transport properties in all junctions are computed within a first-principles Landauer formalism using a scattering-state approach (SCARLET code).[12] All calculations are performed in the zero bias voltage limit. Since the DFT-GGA Kohn−Sham eigenvalues are poor approximations for quasiparticle energies associated with molecular resonances in the junction,[28] we add a

self-energy operator to the DFT-GGA scattering-state Hamiltonian, of the form $\hat{\Sigma} = \sum_n \Sigma_n |\psi_n^{mol}\rangle\langle\psi_n^{mol}|$, where $|\psi_n^{mol}\rangle$ denotes an eigenstate of the isolated molecule, and Σ_n is the self-energy correction for the nth molecular level.[21,22] The transmission spectrum is generated by solving the modified scattering-state Hamiltonian in a "one-shot" calculation (DFT+Σ).

The self-energy correction Σ_n is computed as described in the Methods section. Briefly, the self-energy correction consists of two parts: first, a "molecular" term representing the self-energy correction in the gas-phase molecule; and second, an "image-charge" term[29] accounting for the effect of electrode polarization from both electrodes. When applied to benzenediamine (BDA) and derivatives on Au(111), this self-energy correction predicted highest occupied molecular orbital (HOMO) energies within 0.2 eV of high-resolution photoemission measurements.[30] For the junctions considered here, the gas-phase correction to the HOMO ranges from approximately -2 to -3 eV, while the image charge term reduces the magnitude of this correction significantly, by ~0.7 to 1 eV,[21] depending on the length of the molecule and its orientation in the junction (Supporting Information Table 1).

As described below, S is a derivative of ln $\tau(E)$ with respect to energy (eq 1), where $\tau(E)$ is the electron transmission at energy E. S is therefore much more sensitive than G (which is proportional to $\tau(E)$) to small numerical oscillations in $\tau(E)$ resulting from finite sampling of the $k_\parallel$ grid. While the conductance G was converged with an 8×8 $k_\parallel$-mesh,[21] a 24×24 mesh is used for the thermopower calculations.[31]

The thermopower S is computed from the transmission $\tau(E)$ through the junctions using the following expression:[7,8]

$$S = -\frac{\pi^2 k_B^2 T}{3e}\frac{\partial \ln(\tau(E))}{\partial E}\bigg|_{E=E_F} \equiv -S_0\frac{\partial \ln(\tau(E))}{\partial E}\bigg|_{E=E_F} \quad (1)$$

where T is the mean temperature of the contacts (300 K in the experiment[4] and in these calculations), and $S_0 > 0$. Equation 1 assumes that $\tau(E)$ varies smoothly for $|E - E_F| < k_BT$ and that the temperature gradient ΔT across the junction is small compared to T.[7,8] Both assumptions hold for the systems studied here ($k_BT \sim$ 0.026 eV and $|\Delta T| < 15$ K in the experiments[4]). Moreover, since the measured voltage drop ΔV is found to be linear with ΔT for the small values of ΔT in the experiments, the steady-state scattering formalism is also valid.[4]

In Figure 1b, we show computed transmission functions for DFT and DFT+Σ for two different BDA−Au junctions. The DFT+Σ transmission has additional features[21] at approximately -1.5 to -2 eV that result from hybridization of the HOMO with Au d states at undercoordinated binding sites. By considering Figure 1b and eq 1, we can draw several conclusions. First, the HOMO resonance level is positioned ~1 eV below E_F in DFT-GGA but ~3 eV below E_F in DFT+Σ. The shallower HOMO resonance in DFT-GGA not only results in smaller tunneling barriers at E_F (and therefore larger G) but also gives rise to a steeper slope for ln $\tau(E)$ at E_F. We therefore expect that DFT-GGA will yield larger values for S compared to DFT+Σ. However, the difference between DFT and DFT+Σ values for S may not be as large as those for G because the slope of ln $\tau(E)$ at E_F is less affected by the level alignment than the value of $G = (2e^2/h)\tau(E_F) \equiv G_0\tau(E_F)$. Second, we note that there is an additional shoulder centered at ~-0.3 eV for transmission functions associated with the adatom junction geometries. (The shoulder is absent in the trimer junction geometries.) This shoulder is due to the HOMO hybridizing with Au adatom d states in this energy range.[17] While these features $\tau(E)$ arising from localized adatom d states actually result in a *smaller* difference in G between adatom and trimer junctions,[17] they lead to a steeper slope for ln $\tau(E)$ at E_F than in the trimer junctions, suggesting that S is more sensitive to contact geometry than G.

The conductance in oligophenyldiamine−Au junctions[23] is known to be consistent with off-resonant tunneling, where $G = A\exp(-\beta^G N)$ and $\beta^G = 1.7$ in both DFT+Σ calculations[21] and experiment. Our calculations also indicated that the relation $\tau(E) = A(E)\exp(-\beta^G(E)N)$ holds close to E_F (away from the molecular resonances).[21] Using this expression in eq 1 then implies that

$$S = -S_0\left(\frac{\partial \ln(A(E))}{\partial E}\bigg|_{E=E_F} - \frac{\partial(\beta^G(E))}{\partial E}\bigg|_{E=E_F} N\right) \equiv S_C + \beta^S N \quad (2)$$

where $\beta^S = S_0(\partial(\beta^G(E)))/(\partial E)|_{E=E_F}$, that is, S varies linearly with N, as observed in experiment.[4] Interestingly, the rate of change of S with N, β^S, is proportional to the gradient of β^G evaluated at E_F. The plots of $\beta^G(E)$ in Figure 1c suggest that, for oligophenyldiamine−Au junctions, we expect β^S to be positive and to be larger within DFT-GGA than DFT+Σ. $\beta^G(E)$ is inversely proportional to the decay length of the evanescent states within the HOMO−LUMO gap in the junction (LUMO: lowest unoccupied molecular orbital). Away from the resonances, $\beta^G(E)$ is smaller in DFT than in DFT+Σ, reflecting less penetrating evanescent states for wider quasiparticle HOMO−LUMO gaps.[21] A positive β^S indicates that the evanescent states become less penetrating as E increases across E_F, and this is consistent with the hole character of states in this energy range. (As E increases toward the middle of the HOMO−LUMO gap, the tunneling barrier for holes increases.) The smaller DFT+Σ value for β^S compared to DFT reflects the fact that the HOMO is further from E_F in DFT+Σ for the case considered here, so that the decay length of evanescent states near E_F varies less rapidly with energy.

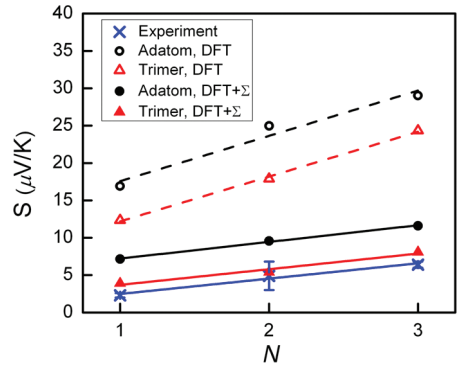

Figure 2. Plot of thermopower *S versus N*. The experimental error bars represent the error in the linear fit for V_{peak} *versus* ΔT^4 and does not take into account the spread in measured voltages at each ΔT.[32]

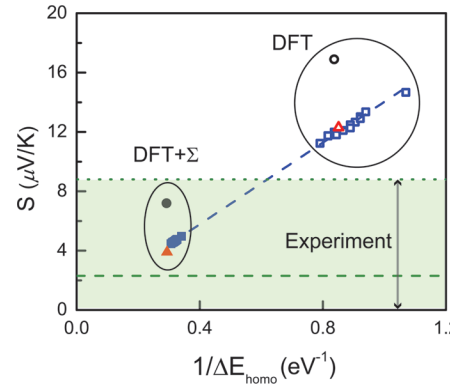

Figure 3. Thermopower *S versus* $1/\Delta E$. Empty blue squares denote values of *S* obtained from Lorentzian fits to DFT transmission for 15 BDA−Au junction geometries ("DFT"),[17] while filled blue squares correspond to *S* obtained from the Lorentzian fits with ΔE increased by 2 eV due to self-energy corrections ("DFT+Σ"). The blue dashed line is a linear fit to the values of *S* obtained from the Lorentzian fits—the gradient of the line is $\approx 2S_0$. Black circles and red triangles denote calculated DFT (empty) and DFT+Σ (filled) values for BDA adatom and trimer junctions, respectively. The green dashed line gives the experimental value for *S* in BDA−Au junctions, while the shaded area denotes the experimental spread ΔS for *S*, obtained by fitting the full width half-maximum of the voltage histograms, V_{fwhm}, *versus* ΔT.[4,32]

We now discuss our computed values of *S* in the context of the above physical arguments and compare our results with experiment (Figure 2 and Table 1). We see that, for each junction, DFT-GGA overestimates *S* while DFT+Σ brings *S* into much better agreement with experiment. For reasons discussed above, the adatom junctions have larger *S* values than the trimer junctions, the latter being in better agreement with the experimentally measured values (Table 1). However, as described below, the DFT+Σ values of *S* for both adatom and trimer junctions are all within the observed experimental spread,[4,32] obtained from the variations in ΔV measured at each ΔT. (Note that this is different from the reported error bar in Table 1, which comes from the goodness of fit for a linear relation between ΔV and ΔT.) In contrast, the DFT-GGA values for *S* are outside of the experimental spread for both binding motifs. Furthermore, comparing the values of β^S with experiment, DFT+Σ yields a β^S value that is almost identical to experiment (2.1 μV/K), while DFT-GGA overestimates β^S by a factor of 3 (6.0 μV/K). The overestimation of *S* and β^S within DFT-GGA is consistent with the HOMO resonance being closer to E_F and with previously reported DFT calculations on oligophenyldithiol−Au junctions.[15] On the other hand, the fact that DFT+Σ gives values of *S* and β^S in good agreement with experiment indicates that eq 1, together with a more rigorous description of junction electronic structure from DFT+Σ, provides an accurate description of charge transport induced by a thermal gradient in these measurements.

TABLE 1. Calculated Values for *G*, *S*, β^G, and β^S in Comparison with Experiment[4,23a]

		DFT	DFT+Σ	Experiment
G (E-3 G_0)	$N = 1$	50.3 (41.3)	5.28 (4.43)	6.40[23]
	$N = 2$	13.6 (11.6)	1.09 (0.832)	1.16[23]
	$N = 3$	3.62 (2.90)	0.179 (0.149)	0.180[23]
S (μV/K)	$N = 1$	12.3 (16.9)	3.9 (7.2)	2.3 ± 0.3[4]
	$N = 2$	17.9 (25.0)	5.4 (9.6)	4.9 ± 1.9[4]
	$N = 3$	24.3 (29.0)	8.1 (11.6)	6.4 ± 0.4[4]
β^G		1.3 ± 0.0	1.7 ± 0.0	1.7 ± 0.1[23]
		(1.3 ± 0.0)	(1.7 ± 0.0)	
β^S (μV/K)		6.0 ± 0.3	2.1 ± 0.3	2.1 ± 0.4[4]
		(6.1 ± 1.2)	(2.2 ± 0.1)	

[a]The calculated values are given for the trimer junction, with the adatom junction in brackets. The error bars for β^G and β^S are obtained from the least-squares fits to $G = A\exp(-\beta^G N)$ and $S = S_C + \beta^S N$. The error bar for *S* in experiment is reported for the linear fit for V_{peak} *versus* ΔT^4 and does not take into account the spread in measured voltages at each ΔT,[32] which is shown in Figure 3.

The agreement between DFT+Σ and experiment is equally good[21] for *G* and β^G (Table 1). The DFT+Σ values for *G* and *S* are both within the experimental spread,[4,23] while those for β^G and β^S are almost identical to experiment. Interestingly, β^G and β^S are largely insensitive to the junction geometry, suggesting that the junction geometry primarily functions to modulate $\tau(E)$ by a multiplicative factor related to the Au DOS. Thus, although our model geometries may not exactly represent the most common junctions in experiment (corresponding to the experimental histogram peak positions for *G* and *S*), β^G and β^S, which are intrinsic properties of the system, serve as robust quantities for comparison between theory and experiment.

We now discuss the impact of geometry on *S* in relation to the observed spread in experiment. It is instructive to consider first a Lorentzian model for transmission

$$\tau(E) = A\frac{\left(\frac{\Gamma}{2}\right)^2}{\left(\left(\frac{\Gamma}{2}\right)^2 + (E - E_H)^2\right)}$$

and understand the dependence of *S* on the coupling constant Γ and HOMO resonance energy E_H. We have

previously found, based on calculations on 15 junction geometries, that the DFT-GGA HOMO transmission peak for BDA−Au junctions fits well to a Lorentzian function, except for additional features due to Au states at under-coordinated Au sites.[17] The resulting Γ varied from 0.3 to 0.6 eV, and E_H, as computed within DFT-GGA, varied from −0.9 to −1.2 eV. (Note that the good fit to a Lorentzian was found to hold true for BDA−Au but may not be so for other systems.) Substituting the Lorentzian expression for transmission into the formula for S gives

$$S = S_0 \frac{2\Delta E_H}{\left(\frac{\Gamma}{2}\right)^2 + (\Delta E_H)^2}$$

where $\Delta E_H = E_F - E_H$. Since in this case $(\Gamma/2)^2 \ll (\Delta E_H)^2$, we may simplify this expression, giving

$$S \approx \frac{2S_0}{\Delta E_H} \quad (3)$$

In Figure 3, we plot estimated DFT and DFT+Σ values of S for the 15 junction geometries in ref 17, using the fitted values of Γ and E_H in expression 3. For the DFT+Σ estimate, we add 2 eV to ΔE_H and assume for simplicity that Γ remains unchanged (2 eV is an average self-energy correction computed for BDA−Au junctions). Within the Lorentzian model, where a single molecular level is interacting with a uniform Au DOS, both Γ and the variations in ΔE_H and Γ remain unchanged for a deeper HOMO level.

Figure 3 has several interesting features. First, the values of S estimated from Lorentzian fits to the transmission follow closely the relation $S \approx (2S_0/\Delta E_H)$, reflecting the fact that $(\Gamma/2)^2 \ll (\Delta E_H)^2$. As a result, since $\Delta E_H \sim 1$ eV in DFT-GGA and ~3 eV in DFT+Σ, the DFT estimates for S are about 3 times larger than those with DFT+Σ. Since $G = G_0\tau(E_F) \approx G_0(A(\Gamma/2)^2)/(\Delta E_H)^2$ under the same approximations, the error in ΔE_H results in a larger difference between DFT and DFT+Σ estimates for G than for S. Second, all the DFT+Σ estimates fall within the experimentally measured spread, while all the DFT estimates are outside of it. Third, the variation in DFT+Σ values is very small (~0.5 eV) compared to the experimental spread. This small variation suggests that the observed spread in measured S values cannot be explained by variations in ΔE_H and Γ within the Lorentzian model. Fourth, revisiting the actual calculated thermopower values for the trimer and adatom junctions (Table 1, red and black points in Figure 3), we see that, for both DFT and DFT+Σ, the computed S values for the trimer junction are within the distribution of the Lorentzian estimates, while the adatom values are significantly larger. This is consistent with the fact that the DFT transmission for the trimer junction fits well to a Lorentzian function, whereas that for the adatom junction does not;[17] the additional shoulder close to E_F for adatom junctions increases S. These results suggest that the experimental spread is likely to arise from additional features in the transmission function that arise from a non-uniform Au DOS, for example, contributions from Au d states related to under-coordinated Au contact atoms, which are different for different samples.

In conclusion, we have used a self-energy corrected approach (DFT+Σ) to compute the thermopower S of oligophenyldiamine−Au junctions. This approach takes into account, without adjustable parameters, many-electron effects in the renormalization of the molecular level alignments at the junction obtained from Kohn−Sham eigenvalues and gives S values in good agreement with experiment.[4,23] Further, the variation of S with the number of phenyl rings N, as quantified by the constant β^S, is predicted by DFT+Σ to be identical to experiment.[4,23] We demonstrate and explain that many-electron self-energy corrections are important for describing S and also account for the observed experimental spread in S. Together with the excellent agreement obtained for G and β^G, as found in our previous studies,[21] our results show that, for oligophenyldiamine−Au junctions, the measured thermopower and conductance, two distinct and *independent* probes of transport, obtained in independent experimental setups, are consistent with each other and with the physics of off-resonant tunneling as captured by the DFT+Σ approach. These results are a strong validation of our approach and of the independent experiments. Moreover, they are of particular value in a field that has traditionally been plagued by a lack of agreement between different types of experiments[10,13] and between experiment and theory.[11,12]

METHODS

This section expands on the description of our theoretical approach that is provided in the main text.

Our density-functional calculations are performed using the generalized gradient approximation (GGA-PBE),[25] as implemented in the SIESTA code.[26] An optimized single-ς basis set is used for the Au *d* shell; all other orbitals are described by double-ς polarization basis sets. Using this basis, the work function for Au(111) was calculated to be within 0.1 eV of experiment, and the HOMO energies of BDA on Au(111) were within 0.1 eV of plane wave calculations (with the VASP code[33]). Geometry optimization was performed using slabs of six Au layers on each side of the molecule and a supercell with 16 Au atoms per layer. All atoms in the molecule and Au atoms up to and including the third layer from either surface were relaxed until the forces on them were <0.05 eV/Å. The distance between the Au slabs was also allowed to relax for the junctions considered here. Γ-point sampling of the supercell Brillouin zone is sufficient for accurate geometry optimizations.

The transmission is obtained using a coherent elastic scattering-state approach within the Landauer formalism, as implemented in the SCARLET code.[12] The junction is divided

into three regions: left bulk, center resistive region (including 4 Au layers on either side of the molecule), and right bulk. The center region is chosen large enough for the Hartree potentials at its boundaries to smoothly match those of the bulk. The bulk regions are infinitely extended away from the junction to simulate open boundary conditions. We note that using localized orbitals to describe transport properties in this study is adequate because tunneling is primarily "through-molecule" rather than "through-space": replacing the BDA molecule with ghost orbitals results in transmission that is orders of magnitude smaller. Energy- and $\mathbf{k}_\parallel$-dependent scattering states are constructed with incoming and outgoing itinerant and evanescent states determined from the bulk Au complex band structure. The energy grid spacing used in this work is 10 meV. The DFT-PBE charge density is first computed (with semi-infinite boundary conditions), using a 4×4 Monkhorst-Pack $\mathbf{k}_\parallel$-mesh to sample the two-dimensional supercell Brillouin zone. Next, the self-energy correction term, $\hat{\Sigma} = \sum_n \Sigma_n |\psi_n^{mol}\rangle\langle\psi_n^{mol}|$, is added to the scattering-state Hamiltonian, where $|\psi_n^{mol}\rangle$ denotes an eigenstate of the isolated molecule, and Σ_n is the self-energy correction for the nth molecular level,[21,22] computed as described below. This scattering-state Hamiltonian is then solved using the DFT charge density as input, and using a denser $\mathbf{k}_\parallel$-mesh (see main text), giving the self-energy corrected scattering states in a one-shot calculation (DFT+Σ).

Since transmission at and near E_F is dominated by the HOMO for the present systems,[21] we compute Σ_n for only the HOMO and LUMO and apply Σ_{HOMO} (Σ_{LUMO}) to all occupied (unoccupied) states. Σ_{HOMO} and Σ_{LUMO} are calculated without adjustable parameters using a physically motivated model that consists of two parts: first, a "molecular" term correcting for the difference between DFT HOMO and LUMO energies and, respectively, the ionization potential (IP) and electron affinity (EA) of the gas-phase molecule computed from total energy differences;[34] and second, an "image-charge" term[29] accounting for the effect of electrode polarization on the energy of the added electron (LUMO) or hole (HOMO), which is calculated from the charge distribution of the LUMO or HOMO, respectively, and includes polarization effects from both electrodes. The IP and EA are computed using the Gaussian program with B3LYP exchange-correlation functional and 6-311g++dp basis set),[35] which gives an IP for BDA to be within 0.1 eV of experiment. For the calculation of the image charge, we assume the electrodes are perfect conductors and take the image plane to be 1 Å from the metal surfaces.[29] Both electrodes are accounted for in the image charge calculation; as a result, each image interacts with an infinite set of images arising from itself, as well as from the other images. To simplify the calculation of the contribution from image charges, the charge distributions associated with frontier orbitals are approximated by Mulliken charges. For smaller molecules like BDA, it is found that even a single point charge in the middle of the molecule results in a reasonable image charge correction term, within 0.1 eV of that obtained from the Mulliken charges. We note that, in this approach, we neglect self-energy corrections to the Au metallic states, which are expected to be much smaller than for states localized on the molecule.[29] This self-energy correction was first derived for a prototypical physisorbed system, benzene on graphite, where it was found to rigorously reproduce many-electron GW HOMO and LUMO levels.[29] We show in an upcoming publication[22] that our approximate self-energy corrections are also valid for chemisorbed systems involving small, weakly polarizable molecules on metal substrates, if the molecular resonances far from the Fermi level and the system is "weakly coupled" in the sense that the character of the molecule's frontier orbitals are preserved relative to the gas phase, and the resonance widths are narrow (a few tenths of an electronvolt). Furthermore, the "off-diagonal" contributions to the self-energy—with metal and other molecular states—should be negligible. We expect that these conditions are well-satisfied for the junctions in this study and that these self-energy corrections will be accurate within a few tenths of an electronvolt; indeed, when the correction is applied to a closely related system, BDA and derivatives on atomically flat Au(111), the resulting DFT+Σ HOMO energy levels agree remarkably well (within 0.2 eV) with HOMO energy levels determined by high-resolution photoemission experiments.[30]

Acknowledgment. We thank J.A. Malen, P. Doak, K. Baheti, R.A. Segalman, A. Majumdar, and T.D. Tilley for stimulating discussions and for sharing their unpublished data with us. Portions of this work were performed at the Molecular Foundry, Lawrence Berkeley National Laboratory, and were supported by the Office of Science, Office of Basic Energy Sciences, of the U.S. Department of Energy. This work was also supported in part by the Director, Office of Science, Office of Basic Energy Sciences, Division of Materials Sciences and Engineering Division, U.S. Department of Energy under Contract No. DE- AC02-05CH11231. We acknowledge computational resources from NERSC. H.J.C. acknowledges support from NRF of Korea (Grant Nos. 2009-0081204 and R01-2007-000-20922-0).

Supporting Information Available: Supplementary Table 1. This material is available free of charge *via* the Internet at http://pubs.acs.org.

REFERENCES AND NOTES

1. Nitzan, A.; Ratner, M. A. Electron Transport in Molecular Wire Junctions. *Science* **2003**, *300*, 1384–1389.
2. Joachim, C.; Gimzewski, J. K.; Aviram, A. Electronics Using Hybrid-Molecular and Mono-Molecular Devices. *Nature* **2000**, *408*, 541–548.
3. Reddy, P.; Jang, S. Y.; Segalman, R. A.; Majumdar, A. Thermoelectricity in Molecular Junctions. *Science* **2007**, *315*, 1568–1571.
4. Malen, J. A.; Doak, P.; Baheti, K.; Tilley, T. D.; Segalman, R. A.; Majumdar, A. Identifying the Length Dependence of Orbital Alignment and Contact Coupling in Molecular Heterojunctions. *Nano Lett.* **2009**, *9*, 1164–1169.
5. Murphy, P.; Mukerjee, S.; Moore, J. Optimal Thermoelectric Figure of Merit of a Molecular Junction. *Phys. Rev. B* **2008**, *78*, 161406-1–161406-4.
6. Finch, C. M.; Garcia-Suarez, V. M.; Lambert, C. J. Giant Thermopower and Figure of Merit in Single-Molecule Devices. *Phys. Rev. B* **2009**, *79*, 033405-1–033405-4.
7. Butcher, P. N. Thermal and Electrical Transport Formalism for Electronic Microstructures with Many Terminals. *J. Phys.: Condens. Matter* **1990**, *2*, 4869–4878.
8. Paulsson, M.; Datta, S. Thermoelectric Effect in Molecular Electronics. *Phys. Rev. B* **2003**, *67*, 241403-1–241403-4.
9. Ke, S. H.; Yang, M.; Curtarolo, S.; Baranger, H. U. Thermopower of Molecular Junctions: An *Ab Initio* Study. *Nano Lett.* **2009**, *9*, 1011–1014.
10. Reed, M. A.; Zhou, C.; Muller, C. J.; Burgin, T. P.; Tour, J. M. Conductance of a Molecular Junction. *Science* **1997**, *278*, 252–254.
11. Stokbro, K.; Taylor, J.; Brandbyge, M.; Mozos, J. L.; Ordejon, P. Theoretical Study of the Nonlinear Conductance of Dithiol Benzene Coupled to Au(111) Surfaces *via* Thiol and Thiolate Bonds. *Comput. Mater. Sci.* **2003**, *27*, 151–160.
12. Choi, H. J.; Cohen, M. L.; Louie, S. G. First-Principles Scattering-State Approach for Nonlinear Electrical Transport in Nanostructures. *Phys. Rev. B* **2007**, *76*, 155420-1–155420-14.
13. Xiao, X. Y.; Xu, B. Q.; Tao, N. J. Measurement of Single Molecule Conductance: Benzenedithiol and Benzenedimethanethiol. *Nano Lett.* **2004**, *4*, 267–271.
14. Dubi, Y.; Di Ventra, M. Thermoelectric Effects in Nanoscale Junctions. *Nano Lett.* **2009**, *9*, 97–101.
15. Pauly, F.; Viljas, J. K.; Cuevas, J. C. Length-Dependent Conductance and Thermopower in Single-Molecule Junctions of Dithiolated Oligophenylene Derivatives: A Density Functional Study. *Phys. Rev. B* **2008**, *78*, 155119-1–155119-14.
16. Tomfohr, J.; Sankey, O. F. Theoretical Analysis of Electron Transport through Organic Molecules. *J. Chem. Phys.* **2004**, *120*, 1542–1554.
17. Quek, S. Y.; Venkataraman, L.; Choi, H. J.; Louie, S. G.; Hybertsen, M. S.; Neaton, J. B. Amine−Gold Linked Single-Molecule Junctions: Experiment and Theory. *Nano Lett.* **2007**, *7*, 3477–3482.

18. Darancet, P.; Ferretti, A.; Mayou, D.; Olevano, V. *Ab Initio* GW Electron−Electron Interaction Effects in Quantum Transport. *Phys. Rev. B* **2007**, *75*, 075102-1–075102-4.
19. Koentopp, M.; Burke, K.; Evers, F. Zero-Bias Molecular Electronics: Exchange-Correlation Corrections to Landauer's Formula. *Phys. Rev. B* **2006**, *73*, 121403-1–121403-4.
20. Hybertsen, M. S.; Louie, S. G. Electron Correlation in Semiconductors and Insulators—Band-Gaps and Quasi-Particle Energies. *Phys. Rev. B* **1986**, *34*, 5390–5413.
21. Quek, S. Y.; Choi, H. J.; Louie, S. G.; Neaton, J. B. Length Dependence of Conductance in Aromatic Single-Molecule Junctions. *Nano Lett.* **2009**, *9*, 3949–3953.
22. Quek, S. Y.; Strubbe, D. A.; Choi, H. J.; Louie, S. G.; Neaton, J. B. First Principles Approach to Charge Transport in Single-Molecule Junctions with Self-Energy Corrections. Manuscript in preparation.
23. Venkataraman, L.; Klare, J. E.; Nuckolls, C.; Hybertsen, M. S.; Steigerwald, M. L. Dependence of Single-Molecule Junction Conductance on Molecular Conformation. *Nature* **2006**, *442*, 904–907.
24. Quek, S. Y.; Kamenetska, M.; Steigerwald, M. L.; Choi, H. J.; Louie, S. G.; Hybertsen, M. S.; Neaton, J. B.; Venkataraman, L. Mechanically-Controlled Binary Conductance Switching of a Single-Molecule Junction. *Nat. Nanotechnol.* **2009**, *4*, 230–234.
25. Perdew, J. P.; Burke, K.; Ernzerhof, M. Generalized Gradient Approximation Made Simple. *Phys. Rev. Lett.* **1996**, *77*, 3865–3868.
26. Soler, J. M.; Artacho, E.; Gale, J. D.; Garcia, A.; Junquera, J.; Ordejon, P.; Sanchez-Portal, D. The SIESTA Method for *Ab Initio* Order-N Materials Simulation. *J. Phys.: Condens. Matter* **2002**, *14*, 2745–2779.
27. This is within 1 degree of the thermal average (at 290 K) of the dihedral angle in oligophenyldiamines with one Au atom bonded to each amine group.
28. Neaton, J. B.; Hybertsen, M. S.; Louie, S. G. Renormalization of Molecular Electronic Levels at Metal−Molecule Interfaces. *Phys. Rev. Lett.* **2006**, *97*, 216405.
29. Ferretti, A.; Calzolari, A.; Di Felice, R.; Manghi, F. First-Principles Theoretical Description of Electronic Transport Including Electron-Electron Correlation. *Phys. Rev. B* **2005**, *72*, 125114-1–125114-13.
30. Dell'Angela, M.; Kladnik, G.; Cossaro, A.; Verdini, A.; Kamenetska, M.; Tamblyn, I.; Quek, S. Y.; Neaton, J. B.; Cvetko, D.; Morgante, A.; *et al.* Relating Energy Level Alignment and Amine-Linked Molecule Junction Conductance. *Nano Lett.* **2010**, *10*, 2470–2474.
31. A 24 × 24 mesh yields the same results for S as a 16 × 16 mesh. Further, numerical smoothing of the resulting ln $\tau(E)$ does not change the value of S by more than 1 μV/K.
32. Malen, J. A.; Doak, P.; Baheti, K.; Tilley, T. D.; Majumdar, A.; Segalman, R. A. The Nature of Transport Variations in Molecular Heterojunction Electronics. *Nano Lett.* **2009**, *9*, 3406–3412.
33. Kresse, G.; Furthmuller, J. Efficient Iterative Schemes for *Ab Initio* Total-Energy Calculations Using a Plane-Wave Basis Set. *Phys. Rev. B* **1996**, *54*, 11169.
34. Jones, R. O.; Gunnarsson, O. The Density Functional Formalism, Its Applications and Prospects. *Rev. Mod. Phys.* **1989**, *61*, 689–746.
35. Frisch, M. J.; Trucks, G. W.; Schlegel, H. B.; Scuseria, G. E.; Robb, M. A.; Cheeseman, J. R.; Montgomery, J., J. A.; Vreven, T.; Kudin, K. N.; Burant, J. C. *et al. Gaussian 03*, revision C.02; Gaussian, Inc.: Wallingford CT, 2004.